Probing the local electronic structure of isovalent Bi atoms in InP

Probing the local electronic structure of isovalent Bi atoms in InP

C. M. Krammel,[1] A. R. da Cruz,[1] M. E. Flatté,[1,2,3] M. Roy,[4] P. A. Maksym,[4]
L. Y. Zhang,[5] K. Wang,[6] Y. Y. Li,[6] S. M. Wang,[6,7] and P. M. Koenraad[1]

[1]*Department of Applied Physics, Eindhoven University of Technology, Eindhoven 5612 AZ, The Netherlands*
[2]*Department of Physics and Astronomy, University of Iowa, Iowa City, Iowa 52242, United States of America*
[3]*Institute for Molecular Engineering, University of Chicago, Chicago, Illinois, 60637, United States of America*
[4]*Department of Physics and Astronomy, University of Leicester, University Road, Leicester LE1 7RH, United Kingdom*
[5]*Department of Physics, University of Shanghai, for Science and Technology, Shanghai 200093, China*
[6]*State Key Laboratory of Functional Materials for Informatics, Shanghai Institute of Microsystem and Information Technology, Chinese Academy of Sciences, Shanghai 200050, China*
[7]*Department of Microtechnology and Nanoscience, Chalmers University of Technology, 41296 Göteborg, Sweden*

(Dated: June 6, 2019)

Cross-sectional scanning tunneling microscopy (X-STM) is used to experimentally study the influence of isovalent Bi atoms on the electronic structure of InP. We map the spatial pattern of the Bi impurity state, which originates from Bi atoms down to the sixth layer below the surface, in topographic, filled state X-STM images on the natural {110} cleavage planes. The Bi impurity state has a highly anisotropic bowtie-like structure and extends over several lattice sites. These Bi-induced charge redistributions extend along the ⟨110⟩ directions, which define the bowtie-like structures we observe. Local tight-binding calculations reproduce the experimentally observed spatial structure of the Bi impurity state. In addition, the influence of the Bi atoms on the electronic structure is investigated in scanning tunneling spectroscopy measurements. These measurements show that Bi induces a resonant state in the valence band, which shifts the band edge towards higher energies. This is in good agreement to first principles calculations. Furthermore, we show that the energetic position of the Bi induced resonance and its influence on the onset of the valence band edge depend crucially on the position of the Bi atoms relative to the cleavage plane.

PACS numbers: 68.37.Ef, 81.15.Hi, 71.55.Eq, 66.35.+a
Keywords: scanning tunneling microscopy, molecular beam epitaxy, III-V semiconductors, highly mismatched alloys

I. INTRODUCTION

Alloying conventional binary semiconductor materials with isovalent impurities, which are significantly different from the host in terms of size and electronegativity, provide a range of accessible perturbing features to the electronic structure without changing the local charge carrier density. In these materials, which are known as highly mismatched alloys (HMAs), the electronic structure of the parent material is perturbed by the impurity states leading to unusual electronic and optical properties. Prominent III-V compound based HMAs are dilute nitrides[1–3] and dilute bismides[4–7]. In these systems, the band anticrossing (BAC) model is successfully used to describe in the dilute limit the influence of highly mismatched isovalent impurities on the band gap and the effective mass of HMAs.[8–10] However, a better understanding of the electronic properties of HMAs beyond the phenomenological level provided by the BAC model requires detailed knowledge of the interactions of the isovalent impurities with each other as well as their host. This has primarily been investigated in a few fundamental works based on tight binding (TB) and density functional theory (DFT) calculations, which involve real-space interpretations of the states introduced into the host by individual N and Bi atoms.[11–15]

Despite many parallels between dilute nitrides and dilute bismides, the nature of the states related to Bi and N dopants differ considerably.[16] However, support from the experimental side for the single-added-atom structure remains minimal; most features seen experimentally emerge for an ensemble of added impurities. Recently cross-sectional scanning tunneling microscopy (X-STM) has been utilized to probe the electronic signatures of single N centers in GaAs.[13,17,18] N creates near the conduction band (CB) a s-like impurity state.[12,14] About dilute III-V-bismides much less is known experimentally, although Bi is expected to introduce a mixed p-like state in the region of the valence band (VB).[14,16] In order to clarify the properties of single Bi atoms within III-V semiconductors, X-STM is used to investigate the electronic structure of the Bi impurity state near the {110} surfaces.

In this paper, we probe the spatial structure of the

Bi impurity state in cleaved {110} InP surfaces. This is done in an approach where filled state X-STM images for Bi atoms down to the sixth layer below the cleavage plane are analyzed. The spatial structure of the experimentally observed Bi impurity state is compared to the spatial structure obtained in the TB calculations for Bi in InP. We find a much shorter ranged perturbation of the valence band of InP relative to that calculated previously for Bi in GaAs.[14] We use scanning tunneling spectroscopy (STS) to investigate the local density of states (LDOS) of the Bi impurity states as a function of energy for Bi atoms at various depth below the surface.

II. EXPERIMENTAL AND COMPUTATIONAL METHODS

The investigated sample contains three different Bi:InP(15 nm)/InP(20 nm) quantum wells (QWs) with Bi concentrations of 0.1 % (QW 1), 0.5 % (QW 2) and 1.0 % (QW 3). Every QW (1, 2, 3) is repeated three times to increase the likelihood of a clean and flat area without atomic steps. The three different sets of identical QWs are separated by 100 nm thick InP spacer layers. The QW region is terminated by a 50 nm thick InP layer, which is followed by a 150 nm InP:Bi bulk layer with a Bi concentration of 2.4%. This protects the QW region and allows easy orientation of the sample. Details of the growth of this samples can be found in an earlier work in which the same sample was investigated.[19]

The X-STM measurements were performed in a commercial Omicron low temperature STM at 5 K. The samples were cleaved under ultra high vacuum (UHV) conditions in the STM chamber at pressures below 4×10^{-11} mbar. Polycrystalline tungsten tips, which were electrochemically etched and further refined in the STM by Ar sputtering, were used as probes. All images were acquired in constant current mode at negative sample voltage. In this regime the tunneling current is dominated by the filled states in the VB, which are primarily associated with group V elements, such as P and Bi.[20]

To calculate the local density of states (LDOS) corresponding to the Bi atom we employed the Koster-Slater Green's function formalism[21] applied to a local defect[22,23] using a bulk $sp^3d^5s^*$ empirical tight-binding Hamiltonian[24] to describe the InP host. Results from this calculation method have been compared previously to STM measurements of single impurities in III-V zinc-blende semiconductor hosts (e.g. Mn in GaAs[25] and N in GaAs[18]) showing good agreement. In our approach the substitutional impurity potential is set by including on site energies equal to the difference in s, p and d atomic energy levels between bismuth and phosphorus, which are obtained from atomic spectra data.[26] The bond distance between the Bi and its four nearest-neighboring In atoms is set by tuning the hopping parameters according to scaling laws described by Jancu. et. al[24] by fitting strained bulk electronic structures. This allowed us to place the bismuth resonance level at 120 meV below the valence band edge as estimated from previous calculations.[27] The distance of the Bi-In bond is 35.3 % longer than a bulk P-In bond.

III. RESULTS AND DISCUSSION

A. Spatial structure of Bi impurity states

We use the ability of the STM to probe the LDOS at the atomic level to explore in conventional topographic filled state X-STM images the spatial structure of the Bi impurity state. This is complicated by the additional dependency of the tunnel current, I_T, on the real topography of the sample. In earlier work we have shown that the geometrical structure of the relaxed surface is considerably modified by Bi atoms down to the second layer below the cleavage plane.[19,28] Therefore, it is important to make a clear distinction between topographic and electronic contributions from Bi atoms to the X-STM images. First indications on the role of these two effects can be derived from X-STM images of the same area, which are recorded at different sample voltages U_S. Real topographic features affect the tunnel current irrespective of the applied voltage. This is due to the exponential dependence of the tunnel current on the distance. The LDOS of this sample has, in contrast to real topographic features, also a strong energy dependency which appears in the tunnel current only at specific sample voltages. In the case of isovalent Bi atoms in InP we have a resonant impurity state just below the valence band edge (VBE).[10] The Bi impurity state affects the tunnel current primarily at small negative sample voltages, when electrons are mainly extracted from occupied states near the VBE into empty tip states. Therefore, it is sufficient to focus on the negative voltage range in which I_T is determined by the VB band states.

Figure 1 (a) shows a small part of QW 3, which is imaged at a large negative sample voltage of $U_S = -2.6$ V. Here, three different Bi related features can be distinguished (0, 1, 2), which arise from Bi atoms down to the second layer below the surface. The numbering starts with 0, which stands for the cleavage plane. The depth of the Bi atoms is determined on the basis of our earlier work in which we identify Bi atoms in and below cleaved {110} InP surfaces.[19] The same area of QW 3 as in Fig. 1 (a) is imaged in (b) at a reduced negative sample voltage of $U_S = -2.0$ V. The appearance of Bi atoms in the first (1) and second (2) layer below the surface changes considerably at this tunneling condition. For example, two of the four P corrugation maxima, which are affected by a Bi atom in layer (1), are significantly brighter at small negative voltages than at larger voltages. Similarly, the atomic like contrast of Bi atoms in layer (2), which is identified at a large negative voltage, extends at smaller voltages over neighboring sites of the P corrugations. An exception are Bi atoms in the cleavage plane (0) whose

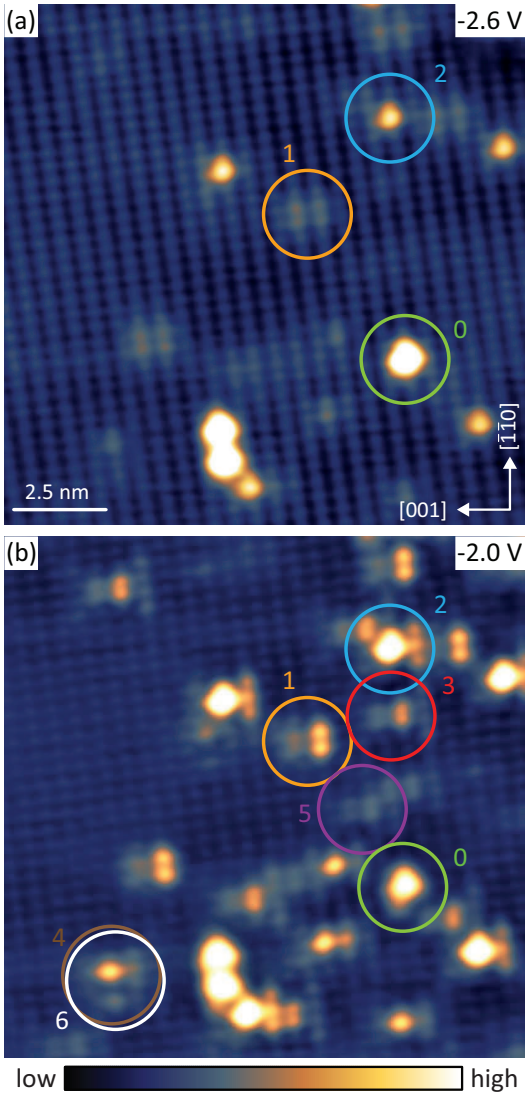

FIG. 1. (Color online) Filled state X-STM images of exactly the same region of QW 3, which are acquired at a tunnel current set point of $I_T = 30$ pA. The X-STM image in (a) is taken at a large negative sample voltage of $U_S = -2.6$ V, where states deep in the VB are probed. In this case, Bi atoms in the first three surface layers (0, 1, 2) are clearly visible. The X-STM image in (b) is taken at a small negative sample voltage of $U_S = -2.0$ V, where states closer to the VBE are probed. This results in a change of the appearance of the Bi atoms in layers (1) and (2). In addition, Bi atoms in deeper layers (3, 4, 5, 6) become visible. The color scales of both images (a, b) are independently adjusted for best visibility. The crystal directions are indicated in (a).

contrast is hardly affected. In addition, previously unseen features, which are marked with numbered circles (3, 4, 5, 6), become visible. These features can only be found in the Bi doped regions, which points towards impurity states of Bi atoms deep below the second layer (e.g. 3, 4, 5, 6). The classification of these new Bi related features is explained in more detail later in this section.

Bi atoms below layer (2) are hardly visible in Fig. 1 (a), which is taken at a large negative voltage where states deep in the VB far away from the Bi impurity state contribute most to the tunnel current. This illustrates that the geometric structure of the surface is primarily affected by Bi atoms down to the second layer (2) below the surface. Similarly, DFT calculations on the structural properties of Bi in InP show that the effectively larger Bi atoms give rise to a short ranged deformation extending only over a few lattice sites in the surrounding InP matrix.[19,28] In contrast, the strong change in the appearance of the Bi atoms in layers (1) and (2) at a smaller negative sample voltage points to considerable contributions from the Bi impurity states in addition to the previously mentioned structural effects on the {110} surfaces. Ultimately, the increased depth sensitivity, when addressing states close the VBE, underlines that the contrast of the new Bi related features in layers 3, 4, 5, and 6 is almost entirely defined by the Bi defect state itself. An example of the sample bias-dependent evolution of the impurity state of a Bi atom in the third layer (3) is provided in section 1 of the supplementary materials. Structural effects prevail for Bi atoms in the surface layer (0), whose appearance is not affected in the studied negative sample voltage range.

High resolution filled state X-STM images of the Bi impurity state, which originate from Bi atoms down to the sixth layer below the $(\bar{1}10)$ InP cleavage plane, are shown in Fig. 2 (a). These maps taken under constant-current conditions resemble cuts along the cleavage plane through the three dimensional Bi defect state, which are displaced by integer numbers of atomic layers (0, 1, 2, 3, 4, 5, 6) from the Bi atom. The Bi defect state displays, except for a Bi atom in the surface (0), a highly anisotropic structure, resembling the bowtie-like contrasts reported for deep acceptor wave functions in zinc-blende III-V compounds.[25,29] However, acceptors such as Mn in GaAs, for which bowtie-like contrasts have been observed at an (110) cleavage plane, always induce a localized state in the bandgap. In contrast to this, Bi in InP is an isovalent impurity, which gives rise to a resonant state outside the bandgap just below the VBE.

The Bi impurity state is similar to deep acceptor states in that it is mirror symmetric in the $(\bar{1}\bar{1}0)$ plane. In the perpendicular directions, along the [001] directions, the observed symmetry of the Bi impurity states is broken. Height profiles, which cut through the highest point of the Bi impurity states in Fig. 2 (a), are provided in Fig. 2 of the supplementary materials. The Bi impurity states can be divided into two types, which have their symmetry center either on or in-between the corrugation of the group V sublattice as indicated by reference lines in the first and second row of Fig. 2 (a). Sketches of these two configurations are provided in Fig. 2 (b) with respect to the underlying lattice. This points, in good agreement with our earlier work,[19] to Bi atoms being incorporated at substitutional P sites in even or odd numbered layers as shown in Fig. 2 (c). Bi is known to substitute for

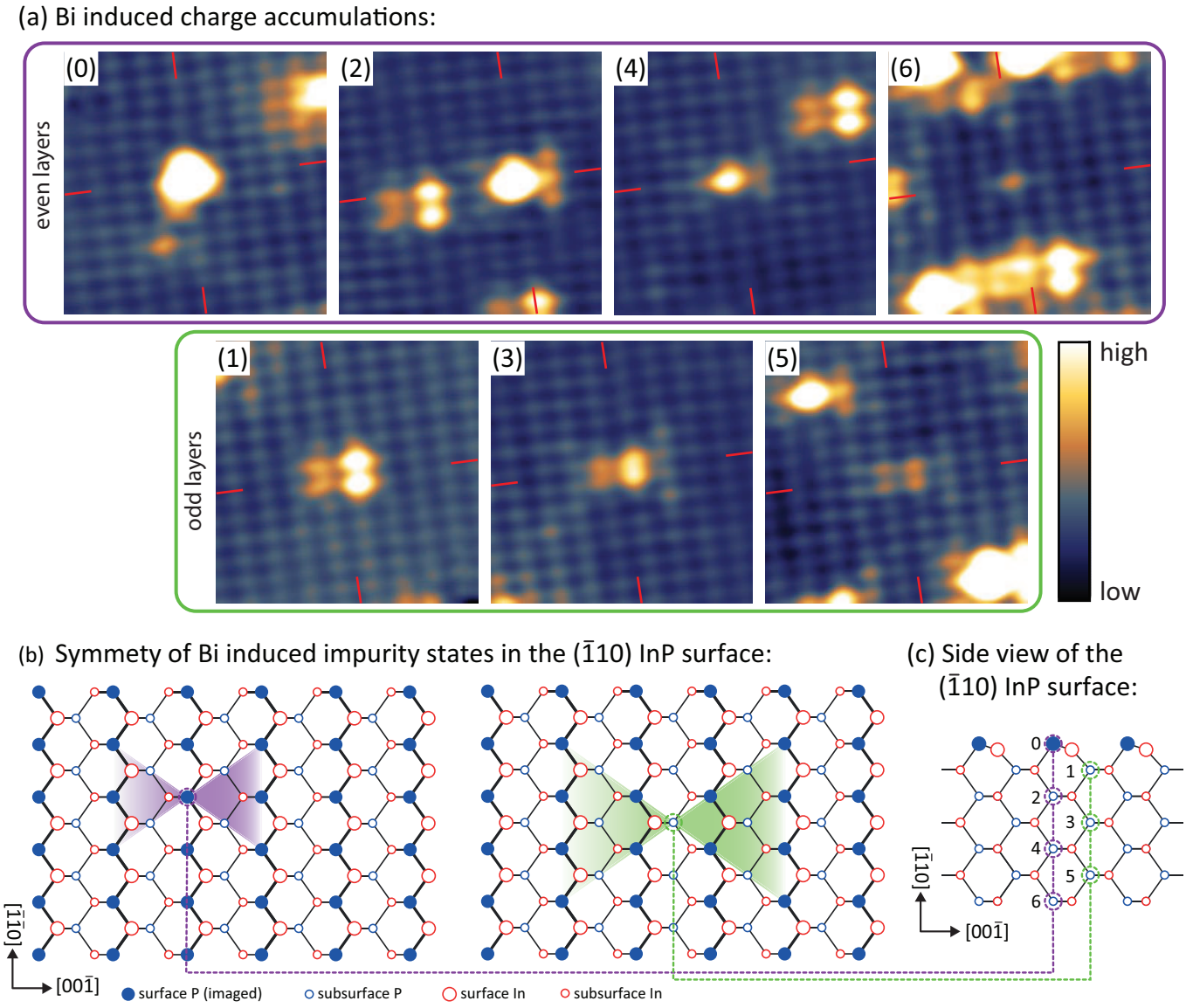

FIG. 2. (Color online) High resolution filled state X-STM images (a) of charge accumulations around individual Bi atoms in the first seven layers (0, 1, ..., 6) of the (1̄10) InP surface (c). The reference lines indicate the center of the Bi related features, which lie for Bi atoms in odd or even numbed layers on or in between the anion sublattice. All images are extracted from a large scale X-STM image of QW 3, which is taken at a tunnel current set point of $I_T = 40$ pA and a sample voltage of $U_S = -2.4$ V. The color scales are independently adjusted to emphasize the spatial structure of the weaker features. The maximum extent of the charge accumulations around the Bi atoms in even and odd layers are shown in the top views of the imaged (1̄10) InP surface (b). Here, filled blue discs represent the group V sublattice, which is probed in filled state X-STM images (a). The positions of the Bi atoms in (a) are indicated in the side view of the relaxed (1̄10) surface (c).

group V lattice positions in III-V compounds with zinc-blende structure, which are grown under group V rich conditions[6]. This allows us to attribute the new Bi related features based on the location of their symmetry center with respect to the group V sublattice in combination with their height in the STM image, which is expected to decrease with increasing distance from the surface, to Bi atoms on P sites between the third (3) and sixth (6) layer. Similarly, the maximum extension of the Bi impurity state increases along the [001] and [1̄1̄0] directions in the (1̄10) surface by an additional lattice site when going from the surface (0) down to the third layer (3). The coupling of Bi atoms in odd numbered layers to the surface is notably stronger than for Bi atoms in even numbered layers, as can be seen in Fig. 2 of the supplementary material. All this suggests that the strongly coupled zigzag rows of In and P atoms along the ⟨110⟩ directions play an important role for the appearance of

the Bi impurity states. An further increase of lateral extension of the impurity state is not observed beyond the third layer (3) below the cleavage surface.

In Fig. 3 we compare the measured contrasts for filled states X-STM images shown in Fig.3 (a) to our tight-binding calculations for the LDOS of Bi atoms, shown in Fig. 3 (b). Previous work has shown that such calculations give a very good approximation of defect states near the cleavage surface.[25,29] The calculations and measurements are shown for the zeroth layer, corresponding to the $(\bar{1}10)$ cleavage plane, and the second and third layers below it. The spatial distribution of the LDOS at each atomic site was obtained by assuming a Gaussian orbital whose width is 1.13 Å, approximately half the distance between an In and its neighboring P atom. Features at smaller length scales could be characterized by the convolution between tip orbitals and surface orbitals but these features are not crucial to compare with the obtained X-STM images. All calculated results were obtained for a resonant state at 120 meV below the VBE with an assumed STM tip width of 1.13 Å. At the (110) surface of III-V semiconductors a surface relaxation induced strain is responsible for the breaking of the mirror symmetry for acceptors, *i.e.*, along the [001] direction for Mn dopant wave functions.[30] Even in bulk there is a small symmetry breaking effect in the (001) plane, but this is dwarfed by that induced by the surface strain. Thus our calculations agree well with the measurements as long as the (001) reflection plane symmetry is (mostly) conserved, as we have not included surface strain in our calculations. The prominent deviations from experiment in Fig. 4 (a,b) in layers 1 and 2 are consistent with the previously observed symmetry breaking, as the differences are characterized by a lower contrast symmetry along the [001] direction in the X-STM images than in the calculated LDOS. In the simulation, which is performed for a bulk system, the enhancement of the LDOS by the Bi atoms is approximately symmetric, while in the experiment an asymmetry regarding the (001) plane is seen. This symmetry breaking in the experiment is due to the relaxation of the $(\bar{1}10)$ surface, which deforms the lattice and induces additional strain at the semiconductor-vacuum-interface.[30]

In the following we compare the structure of the Bi defect states in our experiment to calculations for Bi in GaAs.[14] The structural properties of Bi impurity states in GaAs and InP are expected to be similar. For instance, GaAs and InP have the same crystal structure and Bi induces in both material systems resonant states near the VBE.[10] In addition, the macroscopic electronic properties of GaAs and InP, such as the band gap and spin orbit splitting, are affected similarly upon Bi incorporation.[31] When cutting correspondingly along the $(\bar{1}10)$ plane through the center of the isosurface of the Bi impurity state calculated by Virkkala *et al.* one obtains a bar-like feature, which extends along the $[\bar{1}\bar{1}0]$ and [110] directions. This is not consistent with the atomic like contrast, which is seen for a Bi atom in the surface at a negative U_S. Our DFT calculations have shown that in the (110) surface the Bi atoms relax due to their large effective size into an higher position, which lies above the surrounding.[19,28] This structural modification dominates the contrast in the measurement. But also, the semiconductor-vacuum interface itself is known to modify the pattern of localized states.[32,33] Cuts along the $(\bar{1}10)$ plane, which are displaced by integer multiples of one atomic layer from the center of the Bi impurity state, resemble the situation for Bi atoms below the surface. In this case, cross-like features are expected, which extend increasingly along the four equivalent $\langle\bar{1}\bar{1}\bar{1}\rangle$ directions in the $(\bar{1}10)$. The same applies to the growing extensions of the Bi impurity state in the experiment when going from the surface (0) to the third (3) layer. However, the bow-tie-like structures seen in the X-STM measurement point to a much smaller localization of the Bi impurity states along the $\langle 110\rangle$ directions in InP than suggested for GaAs. Below the third layer (3), the dimensions of the Bi impurity states in even and odd numbered layers increase no longer. This could be related to the local nature of the Bi impurity states or a deviation from the preferential localization along the $\langle 110\rangle$ directions at larger distances.

The global electronic properties of highly mismatched III-V-bismides, such as the band gap and spin orbit coupling, do not solely depend on the interactions between the Bi impurities and the host material. It has recently been suggested that in addition to perturbations induced by single Bi atoms also Bi-Bi interactions play a crucial role in dilute bismides especially at higher Bi concentrations.[14,15] Figure 1 (b) shows that already in the range of a about 1 % Bi the impurity states of a significant amount of Bi atoms are overlapping. The bowtie-like shape of the impurity state, which is observed for isolated Bi atoms, is also conserved for groups of Bi atoms nearby. This shows that the Bi-Bi interactions are highly anisotropic and the need to carefully address issues regarding coupled Bi atoms. The anisotropy of the Bi-Bi coupling in combination with the preferential formation of Bi pairs and clusters along the $\langle 110\rangle$ directions, which we report in Ref.[19], is expected to have a substantial influence on the strength of the Bi induced VB edge broadening compared to models, which are based on ideal crystals where the Bi atoms are distributed randomly.

B. Bi induced modifications of the electronic structure

To further investigate the electronic properties of the Bi impurity state, differential conductance $dI(U)/dU$ spectra are taken at single Bi atoms down to the fifth layer (5) below the surface. The $dI(U)/dU$ can be seen as an approximation of the LDOS in the sample.[34] We calculate the experimental $dI(U)/dU$ spectra on the basis of $I(V)$ curves, which are afterwards numerically differentiated and smoothed with a Savitzky-Golay filter. The $I(V)$ curves are recorded with an open feedback loop af-

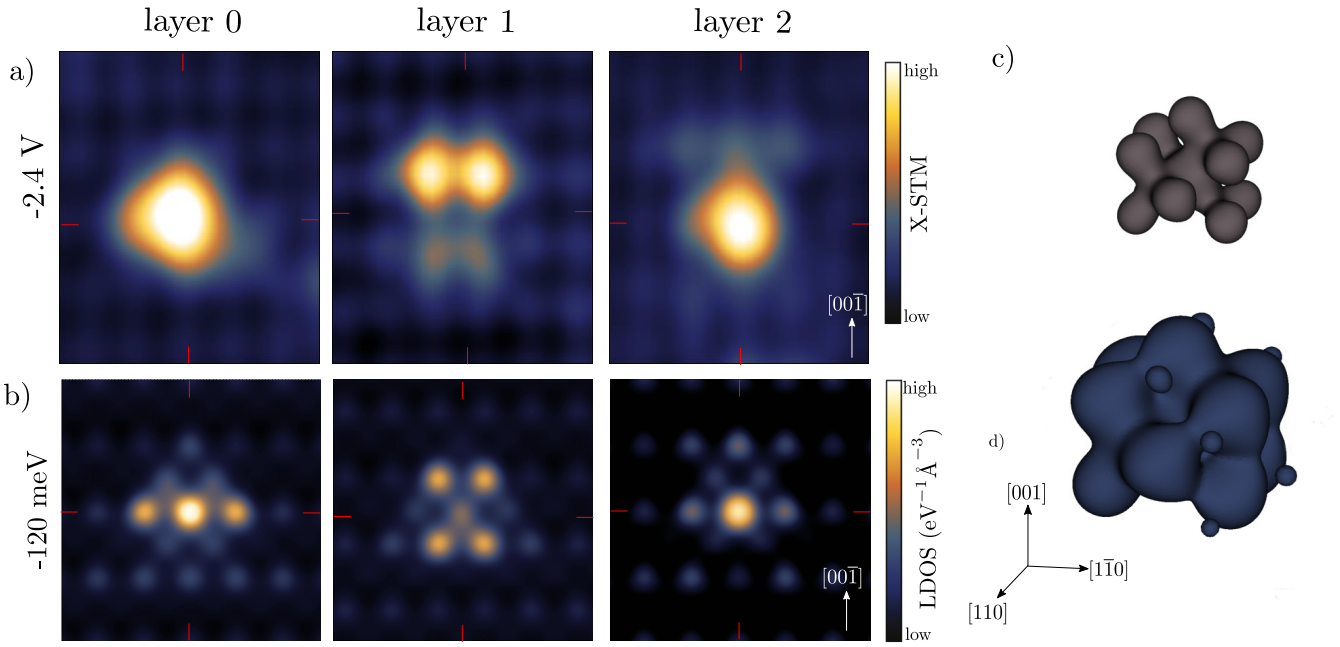

FIG. 3. (a) X-STM measurements of filled states of the ($\bar{1}$10) plane of InP taken at -2.4 V . The layers 0, 1 and 2 correspond to the cleavage surface and the two layers below it respectively. These correspond to the images (0), (1) and (2) of Fig.4 (a). (b) LDOS calculated at 120 meV below the VBE with an assumed STM tip width of 1.13 Å. The red reference lines indicate the location of the Bi atom. (c) and (d) show isodensity surfaces calculated at 120 meV below VBE corresponding to a difference between Bi atom and the background of 0.6 eV^{-1}Å^{-3} and 0.4 eV^{-1}Å^{-3} respectively.

ter having approached the tip by additional 0.16 nm towards the sample. Figure 4 (b) shows typical $dI(U)/dU$ point spectra of individual Bi atoms down to the second layer below the surface and the surrounding InP matrix. These spectra are acquired in the back scan of the STM topograph in Fig. 4 (a), which is based on a tunnel set point of $I_T = 40$ pA and $U_S = -2.4$ V. The onsets of the CB and VB are indicated by dashed vertical lines, which are extracted from a logarithmic plot of the experimental $dI(U)/dU$ curves using a threshold of $t = 0.026$ nA/V. Complementary $dI(U)/dU$ spectra of Bi atoms in deeper layers below the surface are provided in Fig. 5. These $dI(U)/dU$ spectra represent averages of the positions of the correspondingly labeled Bi atoms in Fig. 1 (b), which are extracted from an $I(U)$ map. In contrast to Fig. 1 (b) where the I_T is most sensitive to the Bi impurity state is the I(U) map taken at a tunnel set point of $I_T = 30$ pA and $U_S = -2.5$ V. In this voltage range Bi atoms below the second layer (2) are hardly visible, which minimizes topographical interference as far as it is possible in this material system.

The logarithmic scale in Fig. 5, which increases the weight of the weaker data points, shows that four tunneling regimes have to be distinguished.[35] This is characteristic for the investigated sample. Tunneling from filled tip states into empty CB states takes place at positive U_S in region (I). Region (II) reflects the band gap, where no states are available. The shoulder in region (III) originates in an electron current out of a tip induced charge accumulation layer in the CB. This is related to tip induced band bending (TIBB), which pulls the conduction band edge (CBE) below the Fermi level of the sample at negative U_S. The n-type character of the epilayer region, which is common for low temperature grown InP and Bi:InP,[36] favors the early formation of such a charge accumulation layer in the CB. The fact that the tunneling in Region I starts at 0 V is consistent with the n-type character of the grown material. The additional increase in the $dI(U)/dU$ spectra at higher negative U_S in region (IV) is due to contributions from electrons of the VB to the I_T.

The spectra taken at Bi atoms in different layers and the InP matrix agree very well in regions (I, II, III), which are dominated by the LDOS in the CB. This excludes an interaction of the Bi atoms with the CB states. Conversely, the electronic structure of the VB, which is represented by region (IV), is heavily affected by the presence of Bi. Here, specific Bi related resonances are observed, which are not present in the $dI(U)/dU$ spectra of the InP matrix. This reflects the acceptor like nature of the Bi impurity state. The magnitude of the Bi defect states can be judged best with the linear scale used in Fig. 4 (b). Interestingly, the Bi defect states, which originate from Bi atoms at different depth below the surface, do not lie equally deep in the VB as expected for single Bi atoms far away from each other and any interfaces. The

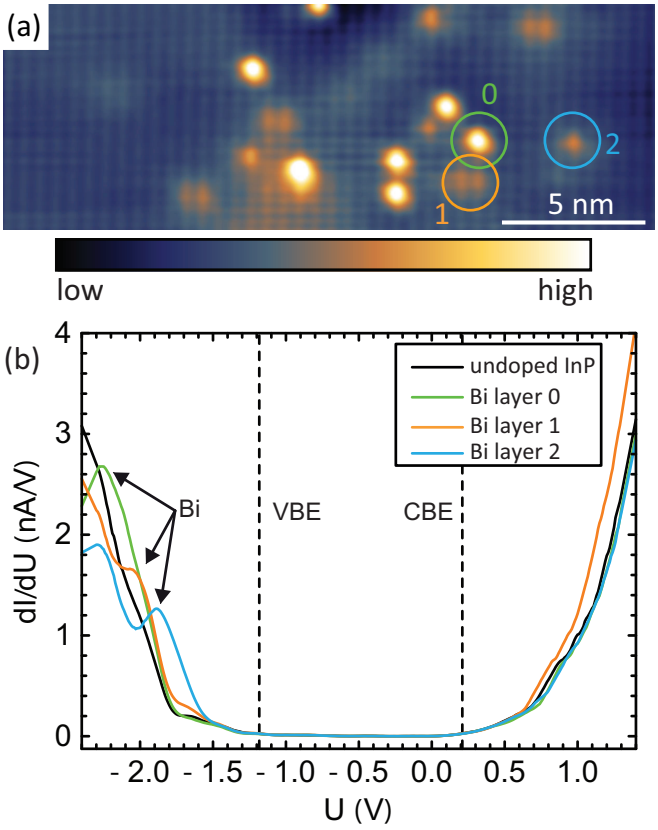

FIG. 4. (Color online) Filled state X-STM image (a) of QW 3 taken at a tunnel current set point of $I_T = 40$ pA and a sample voltage of $U_S = -2.4$ V. The spatially resolved differential conductance spectra $[dI(U)/dU]$ in (b) are taken at Bi atoms down to the second layer below the surface (0, 1, 2), which are marked in (a). A spectrum acquired at the InP matrix (black) serves as a reference. The spectra taken at Bi atoms show in contrast to the InP matrix additional resonances near the VBE, which lie the deeper in the VB the closer the Bi atom is to the surface. The CB and VB edges are indicated by dashed vertical lines.

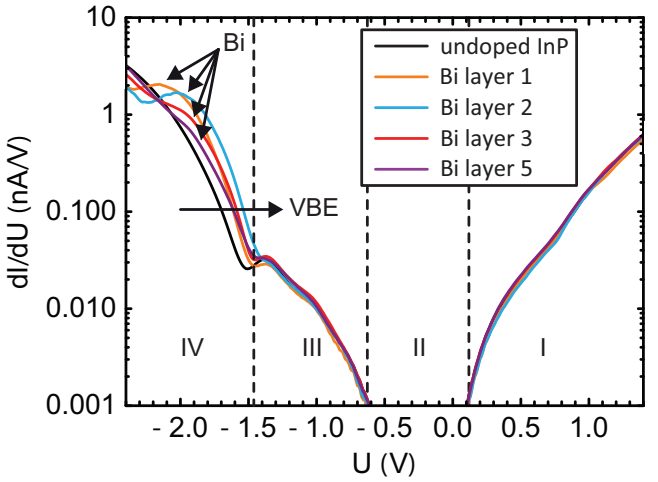

FIG. 5. (Color online) The $dI(U)/dU$ spectra are extracted from a CITS map at the positions of Bi atoms in the first (1), second (2), third (3), and fifth (5) layer, which are labeled accordingly in Fig. 1 (b). A spectrum of the bare InP matrix (black) serves as a reference. A logarithmic scale is used to reveal the VBE, which at the Bi atoms is shifted to higher energies as indicated by an arrow. The tunneling into the VB begins below -1.5 V (IV). The shoulder between -0.6 V and -1.5 V is related to a I_T out of occupied CB states (III). In the band gap (II) tunneling is suppressed. Empty states in the conduction band are addressed at positive U_S (I). The resonant states of Bi atoms in different layers are indicated by fanned arrows.

depth-dependence of the energetic positions of the Bi impurity states in the experimental $dI(U)/dU$ spectra of Figs. 4 (b) and 5 is summarized in Fig. 6. The energetic positions of the Bi impurity states are determined after having subtracted the InP background. In this way we compensate for energy shifts by the superimposed CB states. The error bars represent the full width at half maximum (FWHM) of the Bi states after the background subtraction. The Bi defect states in layers (0, 1, 2) shift with increasing distance from the surface closer to the VBE. This trend is not continued for Bi atoms below the second layer (2) where a stabilization of the Bi impurity state occurs at about (1.9 ± 0.1) V.

It is possible to exclude that the experimentally observed Bi defect states, which are related to Bi atoms in the first three layers (0, 1, 2), are shifted due to changes of the tip state, interactions between Bi atoms close by, or

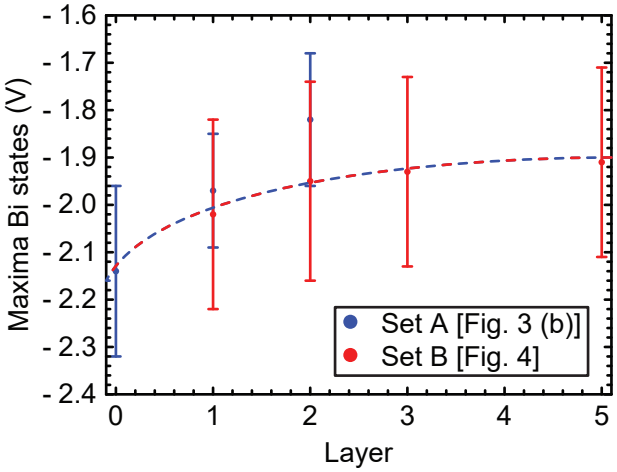

FIG. 6. (Color online) Depth-dependency of the energetic positions of Bi impurity state in the VB. Set A, which is shown in blue, is extracted from the $dI(U)/dU$ spectra in Fig. 4 (b). Set B, which is shown in red, is determined on the basis of the $dI(U)/dU$ spectra in Fig. 5. The energetic positions of the Bi related resonances in the experiment are extracted after subtraction of the InP background. The error bars represent the FWHM of the Bi impurity states.

local potential fluctuations in the surrounding of the Bi atoms. This follows from the observation of corresponding spectral features with different W-tips at Bi atoms, which are further apart from each other than the ones discussed here. In addition, the topography of Bi atoms in the layers (0, 1, 2), which prevails at high negative U_S, leads inevitably to variations in the tip height. This can produce topographic cross talk in the STS spectra due to the additional dependence of the differential conductance on the tip-sample distance. A larger/smaller tip sample distance leads to an underestimate/overestimate of the local density of states (LDOS) and thus to an effectively lower/higher differential conductance.[37] The experimental $dI(U)/dU$ spectra of the InP matrix and Bi atoms agree well at positive voltages, which excludes a strong topographic cross talk. However, when viewing the U-scale of the experimental $dI/dU(U)$ spectra in absolute terms, one has to be cautious. The potential applied between the sample and tip, U_S, partially extends into the semiconductor, which gives rise to tip-induced band bending (TIBB).[38] The TIBB acts as an additional lever, which affects the energy scale in the experimental $dI(U)/dU$ spectra. Similarly, the TIBB, which decays with increasing distance from the surface, can hypothetically lead to an energy shift between Bi impurity states at different depth below the surface. Intrinsic III-V semiconductors have a screening length in the micrometer rage. For degenerate semiconductors the electric field reaches still a few few tens of nanometers into the material. Hence, the TIBB must be very extreme if only Bi atoms in the first three layers (0, 1, 2) below the surface are affected, which appears very unlikely. All this suggest that the energy shift of the Bi impurity states in the first layers goes beyond the level of the naturally occurring TIBB. The influence of the TIBB on the experimental $dI(U)/dU$ spectra is not quantitatively assessed due to lacking information about the probe properties, such as distance of the tip from the sample surface, the actual tip geometry, and the work function of the tip.

It seems likely that the energy shift of the Bi impurity state in layers 0, 1, and 2 is related to the semiconductor-vacuum interface itself. For instance, atoms in the surface have only three bonds to neighboring atoms. The fourth bond is a dangling bond, which is created by the cleavage. This is a completely different situation than in the crystal. In addition, all {110} surfaces of III-V semiconductors with a zinc-blende structure relax with the anions moving outwards and the cations moving inwards, which also influences the arrangement of the atoms in the next lower layer.[39] These structural modifications come along with electronic changes. Similarly, Bi atoms in deeper layers are more constrained by the surrounding lattice, which is increasingly difficult to deform. This leads to growing compressive strain at Bi atoms deeper in the crystal. Under pressure the Bi state is typically shifted deeper into the VB.[16] Another relevant effect is that, the effective dielectric constant of the semiconductor near the surface is expected to be lower than far away from the surface. These effects are strongest near the surface, which fits well to the energetic shift of the Bi impurity states in the first three layers compared to the ones in deeper layers. A similar deepening of the impurity state close to the surface has been reported before[40–42].

Close inspection of the $dI(U)/dU$ curves in Fig. 5 reveals that Bi not only gives rise to a resonance in the VB but also reduces the band gap locally. This is caused by a shift of the VBE in region (IV) to higher energies, which is reflected in an earlier onset of region (IV). A change of the structure of the VB in regions (I) and (III) is not observed. Interestingly, the magnitude of the VB edge extension into the gap varies for Bi atoms at different depth, which we attribute to two effects. On the one hand, the perturbation of the host states decays with growing distance from the Bi atoms. On the other hand, we have shown that the Bi impurity state near the surface is shifted deeper into the VB, which in turn reduces its effect on the VBE. These two opposing effects cause, that the VB edge extension is strongest for a Bi atom in the second layer (2) below the surface. The VBE at the Bi atom in layer (2) is between -1.52 V and -1.85 V on average shifted by $\Delta_{VBE} = (0.21 \pm 0.03)$ V towards higher energies, which has to be seen as a lower limit for the Bi induced lifting of the VBE. The modification of the VBE is expected to be largest directly at the Bi atom, which corresponds to Bi atoms in the surface (1). But this cannot be measured directly due to the additional influence of the surface on the position of the Bi defect state.

Many band models, which predict the influence of Bi on the band gap of III-V semiconductor compounds, suggest that at low Bi concentrations there is a homogeneous shift of the VBE towards higher energies.[10,31,43,44] Our experiment shows the nature of the band gap reduction in these regimes is rather determined by local Bi induced potential fluctuations, which give rise to localization. In contrast to some theoretical work,[31,43,44] which suggest that Bi incorporation affects both the CB and VB, we see at the atomic level no indications for a downward shift of the VB by single Bi atoms. The observation of a Bi related resonance in the VB in combination with the VB edge extension are more in favor of a conventional BAC interaction.

IV. CONCLUSION

In this work, we close the gap between theory, which discusses the perturbation of conventional III-V based semiconductor alloys by isovalent Bi impurities, and experimental observations, which are largely lacking in real space imaging at the atomic level. We address this by utilizing X-STM to investigate the influence of Bi impurities on the charge carrier distribution of InP. We visualize in filled state X-STM images of the natural {110} cleavage plane the depth-dependence of the Bi impurity state. The depth of the Bi actual atoms is determined on the

basis of the symmetry, height, and extensions of the Bi impurity states. Voltage dependent measurements show that topographic modifications of the surface by the effectively larger Bi atoms are only relevant for Bi atoms down to the second layer below the surface. In fact, the Bi impurity state has a highly anisotropic bowtie-like shape and extends over several lattice sites, which points to a strong coupling with the host along to the zigzag rows of In and P atoms in the ⟨110⟩ directions. The structure of the Bi resonant state is well reproduced by tight-binding calculations incorporating the atomic shifts of levels at the Bi impurity, along with a small shift of the Bi-In bond length relative to the bulk P-In bond length. Small discrepancies can be understood as due to the surface strain induced symmetry breaking of the valence state electronic structure.

Complementary STS measures on Bi atoms at different depth below the surface reveal distinct Bi related resonances in the VB and a shift of the band edge towards higher energies. In the first layers (0, 1, 2) near the surface the energetic position of the Bi impurity state further into the conduction band with increasing proximity to the surface. As a result, the displacement of the VBE is with $\Delta_{VBE} = (0.21 \pm 0.03)$ V most pronounced for Bi atoms in the second layer (2) below the surface, which has to be seen as a lower limit for the Bi induced lifting of the VBE.

CMK and PMK thank NanoNextNL, a micro and nanotechnology consortium of the Government of the Netherlands and 130 partners for financial support. LYZ, KW, YYL and SMW wish to acknowledge the National Basic Research Program of China (Grant No. 2014CB643902) and the Key Program of Natural Science Foundation of China (Grant No. 61334004) for financial support. This project has received funding from the European Union's Horizon 2020 research and innovation programme under the Marie Sklodowska-Curie grant agreement No 721394. Contributions to the development of the theoretical calculation by MEF for Bi in InP through modification of hopping matrix elements associated with changes in bond length was supported by the U.S. Department of Energy, Office of Basic Energy Sciences, Division of Materials Sciences and Engineering under Award No. DE-SC0016447.

[1] S. Francoeur, G. Sivaraman, Y. Qiu, S. Nikishin, and H. Temkin, Appl. Phys. Lett. **72**, 1857 (1998).
[2] W. Shan, W. Walukiewicz, K. M. Yu, J. Wu, J. W. A. III, E. E. Haller, H. P. Xin, and C. W. Tu, Appl. Phys. Lett. **76**, 3251 (2000).
[3] W. G. Bi and C. W. Tu, J. Appl. Phys **80**, 1934 (1996).
[4] S. Francoeur, M.-J. Seong, A. Mascarenhas, S. Tixier, M. Adamcyk, and T. Tiedje, Appl. Phys. Lett. **82**, 3874 (2003).
[5] S. P. Svensson, H. Hier, W. L. Sarney, D. Donetsky, D. Wang, and G. Belenky, J. Vac. Sci. Technol. B **30** (2012).
[6] K. Wang, Y. Gu, H. F. Zhou, L. Y. Zhang, C. Z. Kang, M. J. Wu, W. W. Pan, P. F. Lu, Q. Gong, and S. M. Wang, Sci. Rep. **4**, 5449 (2014).
[7] J. Kopaczek, R. Kudrawiec, M. P. Polak, P. Scharoch, M. Birkett, T. D. Veal, K. Wang, Y. Gu, Q. Gong, and S. Wang, Appl. Phys. Lett. **105**, 222104 (2014).
[8] J. Wu, W. Shan, and W. Walukiewicz, Semicond. Sci. Technol. **17**, 860 (2002).
[9] W. Shan, W. Walukiewicz, J. W. Ager, E. E. Haller, J. F. Geisz, D. J. Friedman, J. M. Olson, and S. R. Kurtz, Phys. Rev. Lett. **82**, 1221 (1999).
[10] K. Alberi, J. Wu, W. Walukiewicz, K. M. Yu, O. D. Dubon, S. P. Watkins, C. X. Wang, X. Liu, Y.-J. Cho, and J. Furdyna, Phys. Rev. B **75**, 045203 (2007).
[11] P. R. C. Kent and A. Zunger, Phys. Rev. B **64**, 115208 (2001).
[12] V. Virkkala, V. Havu, F. Tuomisto, and M. J. Puska, Phys. Rev. B **88**, 035204 (2013).
[13] L. Ivanova, H. Eisele, M. P. Vaughan, P. Ebert, A. Lenz, R. Timm, O. Schumann, L. Geelhaar, M. Dähne, S. Fahy, H. Riechert, and E. P. O'Reilly, Phys. Rev. B **82**, 161201 (2010).
[14] V. Virkkala, V. Havu, F. Tuomisto, and M. J. Puska, Phys. Rev. B **88**, 235201 (2013).
[15] L. C. Bannow, O. Rubel, S. C. Badescu, P. Rosenow, J. Hader, J. V. Moloney, R. Tonner, and S. W. Koch, Phys. Rev. B **93**, 205202 (2016).
[16] Y. Zhang, A. Mascarenhas, and L.-W. Wang, Phys. Rev. B **71**, 155201 (2005).
[17] N. Ishida, M. Jo, T. Mano, Y. Sakuma, T. Noda, and D. Fujita, Nanoscale **7**, 16773 (2015).
[18] R. C. Plantenga, V. R. Kortan, T. Kaizu, Y. Harada, T. Kita, M. E. Flatté, and P. M. Koenraad, Phys. Rev. B **96**, 155210 (2017).
[19] C. M. Krammel, M. Roy, F. J. Tilley, P. A. Maksym, L. Y. Zhang, P. Wang, K. Wang, Y. Y. Li, S. M. Wang, and P. M. Koenraad, Phys. Rev. Materials **1**, 034606 (2017).
[20] P. Ebert, B. Engels, P. Richard, K. Schroeder, S. Blügel, C. Domke, M. Heinrich, and K. Urban, Phys. Rev. Lett. **77**, 2997 (1996).
[21] G. F. Koster and J. C. Slater, Phys. Rev. **95**, 1167 (1954).
[22] J.-M. Tang and M. E. Flatté, Phys. Rev. Lett. **92**, 047201 (2004).
[23] V. Kortan, C. Sahin, and M. E. Flatté, Physical Review B **93**, 220402(R) (2016).
[24] J.-M. Jancu, R. Scholz, F. Beltram, and F. Bassani, Phys. Rev. B **57**, 6493 (1998).
[25] A. M. Yakunin, A. Y. Silov, P. M. Koenraad, J. H. Wolter, W. Van Roy, J. De Boeck, J.-M. Tang, and M. E. Flatté, Phys. Rev. Lett. **92**, 216806 (2004).
[26] C. E. Moore and J. E. Mack, Physics Today **5**, 23 (1952).
[27] S. Tiwari and D. J. Frank, Applied Physics Letters **60**, 630 (1992).
[28] F. J. Tilley, M. Roy, P. A. Maksym, P. M. Koenraad, C. M. Krammel, and J. M. Ulloa, Phys. Rev. B **93**, 035313 (2016).

[29] C. Celebi, P. M. Koenraad, A. Y. Silov, W. Van Roy, A. M. Monakhov, J.-M. Tang, and M. E. Flatté, Phys. Rev. B **77**, 075328 (2008).
[30] C. Celebi, J. K. Garleff, A. Y. Silov, A. M. Yakunin, P. M. Koenraad, W. Van Roy, J.-M. Tang, and M. E. Flatté, Phys. Rev. Lett. **104**, 086404 (2010).
[31] M. P. Polak, P. Scharoch, and R. Kudrawiec, Semicond. Sci. Technol. 30 **30**, 094001 (2015).
[32] F. Marczinowski, J. Wiebe, J.-M. Tang, M. E. Flatté, F. Meier, M. Morgenstern, and R. Wiesendanger, Phys. Rev. Lett. **99**, 157202 (2007).
[33] J. K. Garleff, C. Celebi, W. Van Roy, J.-M. Tang, M. E. Flatté, and P. M. Koenraad, Phys. Rev. B **78**, 075313 (2008).
[34] N. D. Lang, Phys. Rev. B **34**, 5947 (1986).
[35] N. Ishida, K. Sueoka, and R. M. Feenstra, Phys. Rev. B **80**, 075320 (2009).
[36] L. Gelczuk, H. Stokowski, J. Kopaczek, L. Zhang, Y. Li, K. Wang, P. Wang, S. Wang, and R. Kudrawiec, J. Phys. D: Appl. Phys. **49**, 115107 (2016).
[37] A. P. Wijnheijmer, O. Makarovsky, J. K. Garleff, L. Eaves, R. P. Campion, B. L. Gallagher, and P. M. Koenraad, Nano Lett. **10**, 4874 (2010).
[38] R. M. Feenstra, Y. Dong, M. P. Semtsiv, and W. T. Masselink, Nanotechnology **18**, 044015 (2007).
[39] J. R. Chelikowsky and M. L. Cohen, Phys. Rev. B **20**, 4150 (1979).
[40] A. P. Wijnheijmer, J. K. Garleff, K. Teichmann, M. Wenderoth, S. Loth, R. G. Ulbrich, P. A. Maksym, M. Roy, and P. M. Koenraad, Phys. Rev. Lett. **102**, 166101 (2009).
[41] T. O. Strandberg, C. M. Canali, and A. H. MacDonald, Phys. Rev. B **81**, 054401 (2010).
[42] J. K. Garleff, A. P. Wijnheijmer, A. Y. Silov, J. van Bree, W. Van Roy, J.-M. Tang, M. E. Flatté, and P. M. Koenraad, Phys. Rev. B **82**, 035303 (2010).
[43] Z. Batool, K. Hild, T. J. C. Hosea, X. Lu, T. Tiedje, and S. J. Sweeney, Journal of Applied Physics **111**, 113108 (2012).
[44] M. Usman, C. A. Broderick, A. Lindsay, and E. P. O'Reilly, Phys. Rev. B **84**, 245202 (2011).